Elasticity of a semiflexible filament with a discontinuous tension due to a cross-link or a molecular motor

Mohammadhosein Razbin,[1,*] Panayotis Benetatos,[2,†] and Annette Zippelius[1]
[1]*Institute for Theoretical Physics, Georg August University, Friedrich-Hund-Platz 1, 37077 Göttingen, Germany*
[2]*Department of Physics, Kyungpook National University, 80 Daehakro, Bukgu, Daegu 702-701, Republic of Korea*
(Received 29 January 2016; revised manuscript received 8 April 2016; published 18 May 2016)

We analyze the stretching elasticity of a wormlike chain with a tension discontinuity resulting from a Hookean spring connecting its backbone to a fixed point. The elasticity of isolated semiflexible filaments has been the subject in a significant body of literature, primarily because of its relevance to the mechanics of biological matter. In real systems, however, these filaments are usually part of supramolecular structures involving cross-linkers or molecular motors, which cause tension discontinuities. Our model is intended as a minimal structural element incorporating such a discontinuity. We obtain analytical results in the weakly bending limit of the filament, concerning its force-extension relation and the response of the two parts in which the filament is divided by the spring. For a small tension discontinuity, the linear response of the filament extension to this discontinuity strongly depends on the external tension. For large external tension f, the spring force contributes a subdominant correction $\sim 1/f^{3/2}$ to the well-known $\sim 1/\sqrt{f}$-dependence of the end-to-end extension.

DOI: 10.1103/PhysRevE.93.052408

I. INTRODUCTION

Over the past couple of decades, it has become clear that mechanics plays a very important role in the biological function of the cell, on a par with biochemistry [1–3]. In order to unravel the physical basis of the complex mechanical behavior of biological matter, a bottom-up strategy has proven very fruitful [4]. In this approach, the basic functional modules of the cytoskeleton are reconstituted *in vitro* and analyzed experimentally in tandem with theoretical modeling.

The basic structural elements of the cytoskeleton (microtubules, intermediate filaments, F-actin) are all semiflexible polymers with a behavior intermediate between that of a random coil and a rigid rod [5,6]. They form supramolecular assemblies (e.g., networks, bundles) through cross-linking [7]. Cross-linking involves a host of different filament-binding proteins [8,9]. Active processes in the cell, such as the delivery of cargos, transport of organelles, mitotic dynamics, as well as muscle contraction are carried out by molecular motors using actin filaments or microtubules as tracks. The bottom-up approach to the study of molecular motors aims at analyzing the transduction of metabolic energy into mechanical force and motion at the microscopic level using *in vitro* assays [10]. The advances in single-molecule manipulation are harnessed to study the simplest motor-filament complexes. In gliding assays, the motor (myosin, kinesin, or dynein) is attached to a glass surface and the translocation of the filament (F-actin or microtubule) is observed. In single motor assays, the filament is attached to the glass surface and the movement of the motor is monitored. In motor assays with beads, the motor is attached to a micron-sized refractile bead whose position is measured [11].

In this paper, we investigate analytically the mechanical response of a semiflexible filament with a tension discontinuity. Our model system can be viewed as one of the simplest structural elements of the cytoskeleton beyond the isolated single-molecule level. We consider a semiflexible polymer, modeled as a wormlike chain, in the weakly bending approximation. The latter can be satisfied either by applying a strong tensile force, which irons out large thermal undulations, or by having a filament with large persistence length compared to its contour length. A longitudinal Hookean spring whose one end is attached to a fixed substrate, has its other end on the filament thus exerting a force that causes the tension discontinuity. The position of one end of the filament is held fixed, whereas that of the other end fluctuates. Its average position yields the force-extension relations, which are the main subject of our analysis. The spring may be viewed as representing a motor, according to the myosin cross-bridge model first introduced by Huxley in 1957 [12] and still in use [13]. Our results apply to passive motors or to very slowly stepping motors, slower than the relaxation time of the filament. The timescale can be tuned by adjusting the concentration of ATP molecules. We should point out, however, that our study of semiflexible filaments with tension discontinuity is also relevant to passive cross-linkers of large size or compliance. Many of the actin binding proteins fall in this category as they can have large spacer domains [7]

Our paper is organized as follows. In Sec. II we introduce the model and show how the discontinuity along the filament contour arises. In Sec. III we discuss the method of Green functions, which allows us to calculate correlation functions of the filament tangent vector and therefore the force-extension relation for different boundary conditions. Explicit results for the case of small spring force, large spring force, and large spring and external forces with a small difference between them are given in Sec. IV. In Sec. V we discuss the relation of our analysis to single-motor experiments. We conclude in Sec. VI, and details of our calculations are given in the Appendices.

II. MODEL DESCRIPTION

Our starting point is the wormlike chain model for a semiflexible filament of contour length L, which is attached to a point or wall on one side and pulled by a constant force, $\mathbf{f}_{\mathbf{ext}}$,

*m.razbin@theorie.physik.uni-goettingen.de
†pben@knu.ac.kr

on the other side. Its Hamiltonian is given by

$$H_{\rm WLC} = \frac{\kappa}{2}\int_0^L \left(\frac{d\mathbf{t}}{ds}\right)^2 - \mathbf{f_{ext}}\int_0^L \frac{d\mathbf{t}}{ds}. \quad (1)$$

Here $\mathbf{t}(s)$ is the tangent vector at arclength s, $0 \leqslant s \leqslant L$, and κ denotes the bending stiffness. We will treat the above model in the weakly bending approximation [14], assuming that the persistence length $l_p = \kappa/(k_B T)$ is much larger than the length L of the filament.

In the Monge parametrization [15], the tangent of a semiflexible filament is given by $\mathbf{t}(s) = \frac{1}{\sqrt{1+a_1^2(s)+a_2^2(s)}}(1,a_1(s),a_2(s))$. We assume that the filament is oriented along the x direction, either due to the grafting on the left side and/or the pulling force $\mathbf{f_{ext}} = f_{\rm ext}\mathbf{e}_x$. In the weakly bending limit the transverse components of the tangent vector $a_1(s)$ and $a_2(s)$ are small. We therefore approximate $t_x(s) = 1 - \frac{1}{2}[a_1^2(s) + a_2^2(s)]$ and $(\frac{d\mathbf{t}(s)}{ds})^2 = \dot{a}_1^2(s) + \dot{a}_2^2(s)$, where the dot denotes the derivative with respect to s. The Hamiltonian then reads

$$H_{\rm WB} = \sum_{i=1}^{2}\left\{\int_0^L \left[\frac{\kappa}{2}\dot{a}_i^2(s) + \frac{f_{\rm ext}}{2}a_i^2(s)\right]ds\right\}. \quad (2)$$

Here, we are interested in the effects of a motor whose one end is grafted to a substrate while the other end is attached to the filament at arclength L_m. In the simplest model, the motor is just a spring of rest length L_0 and spring constant k_m,

$$H_{\rm spring} = \frac{k_m}{2}(R_1 - X_0 - L_0)^2 \quad (3)$$

(see Fig. 1). When the motor steps along the filament, its effective spring is compressed or extended beyond the rest length, resulting in a force, f_m, on the filament. Since the pulling force, $f_{\rm ext}$, is fixed the presence of the motor will result in a compression or extension of the filament. In this paper, we compute the change in the force-extension relation of the filament due to the attached motor.

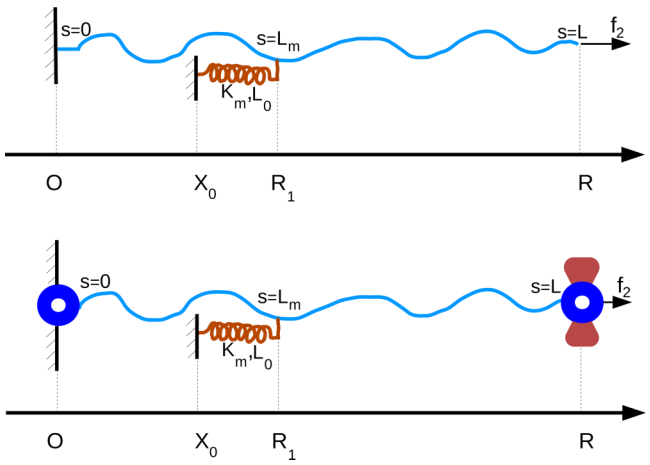

FIG. 1. Schematic presentation of a filament attached to a spring with clamped-free and hinged-hinged boundary conditions at the ends. One end of the spring is fixed to the substrate. The spring pulls one side of the filament and pushes the other side. Therefore, the two sides of the filament are at different tension.

In the weakly bending approximation, we can represent the total Hamiltonian $H = H_{\rm WB} + H_{\rm spring}$ in the form of a filament with an arclength-dependent tension:

$$H = \sum_{i=1}^{2}\left\{\int_0^L \left[\frac{\kappa}{2}\dot{a}_i^2(s) + \frac{f(s)}{2}a_i^2(s)\right]ds\right\}, \quad (4)$$

where $f(s)$ is a piecewise constant function,

$$f(s) = \begin{cases} f_{\rm ext} + f_m & 0 < s < L_m \\ f_{\rm ext} & L_m < s < L \end{cases}, \quad (5)$$

with $f_m = k_m(X_0 - L_m + L_0)$.

Actually, the assumption of a harmonic spring for the motor is not needed as long as we use the weakly bending approximation. Consider a general interaction potential instead, $V(R_1)$. In the weakly bending approximation, we take

$$R_1 - L_m = -\frac{1}{2}\sum_{i=1}^{2}\int_o^{L_m} a_i^2(s)ds \quad (6)$$

to be small, and expand V around $R_1 = L_m$,

$$V(R_1) = V(L_m) + \frac{\partial V}{\partial R_1}(R_1 - L_m) = V(L_m) + \frac{f_m}{2}\sum_{i=1}^{2}\int_0^{L_m} a_i^2(s)ds,$$

resulting in the same effective Hamiltonian [Eq. (4)], but now for a general interaction potential.

We want to compute the end-to-end distance of the filament $\langle R\rangle = \langle x(L) - x(0)\rangle$. To that end, we first calculate

$$\langle R_2\rangle = (L - L_m) - \frac{1}{2}\sum_{i=1}^{2}\int_{L_m}^{L}\langle a_i^2(s)\rangle ds \quad (7)$$

and similarly $\langle R_1\rangle$, where the thermal average $\langle ...\rangle$ is to be taken with the Hamiltonian of Eq. (4).

III. SOLUTION USING GREEN FUNCTION

Using integration by parts for the first term in Eq. (4), we find

$$H_{\rm WB} = \frac{1}{2}\sum_{i=1}^{2}\left[\int_0^L a_i(s)O(s)a_i(s)ds + B_i\right], \quad (8)$$

where $B_i = \frac{\kappa}{2}a_i(s)\dot{a}_i(s)\,|_0^L$ depends on the boundary conditions and is a constant and $O(s) = -\kappa\frac{d^2}{ds^2} + f(s)$ is a differential operator. The corresponding Green function obeys the differential equation

$$\beta\left[-\kappa\frac{d^2}{ds^2} + f(s)\right]G(s,s') = \delta(s - s'). \quad (9)$$

For a piecewise constant force $f(s)$ we can solve for the Green function in the two regions with constant force and then match the solutions at $s = L_m$ (see the Appendix). For the explicit calculation, we have to specify boundary conditions at both ends of the filament. We consider two cases: the clamped-free filament, shown in the upper part of Fig. 1, and the hinged-hinged filament, shown in the lower part of Fig. 1.

A. Clamped-free filament

We require $\dot{a}_i(L) = 0$ at the free end and $a_i(0) = 0$ at the clamped end. For the Green function this implies

$$G_{\rm cf}(s,s')\mid_{s=0} = 0 \quad \frac{\partial}{\partial s} G_{\rm cf}(s,s')\mid_{s=L} = 0. \tag{10}$$

The correlation function of the transverse components of the tangent vector can be obtained from the Green function as follows [16,17]:

$$\langle a_i(s) a_i(s')\rangle = G_{\rm cf}(s,s'). \tag{11}$$

If no motor is attached, the force-extension relation reads [15]

$$\langle R\rangle_{\rm WLC} = \langle R_1 + R_2\rangle = L - \frac{L^2}{2l_p}\left(\frac{\tanh(\tilde{f}_{\rm ext})}{\tilde{f}_{\rm ext}}\right). \tag{12}$$

The characteristic energy scale of the WLC is given by κ/L. Hence, we have rescaled the externally applied pulling force with the bending force of the wormlike chain and introduced $\tilde{f}_{\rm ext} = f_{\rm ext}L^2/\kappa$. We get a linear relation for small forces,

$$f_{\rm ext} = k_{\parallel}^{\rm cf}(L)(L_r - \langle R\rangle), \tag{13}$$

with rest length $L_r = L - L^2/2l_p$ and stiffness $k_{\parallel}^{\rm cf}(L) = \frac{6l_p^2}{\beta L^4}$ [15].

B. Hinged-hinged filament

In this case we require $\dot{a}_i(L) = 0$ and $\dot{a}_i(0) = 0$ implying for the Green function

$$\frac{\partial}{\partial s} G_{\rm hh}(s,s')\mid_{s=0} = 0 \quad \frac{\partial}{\partial s} G_{\rm hh}(s,s')\mid_{s=L} = 0. \tag{14}$$

For a compressive external force $f_{\rm ext}$, the filament is free to rotate at the grafted end. This can be prevented by requiring that the pulling point has to have the same height as the grafting point: $\int_0^L a_i(s) = 0$. The correlation function of the components of the tangent vector is then given by [16,17]

$$\langle a_i(s) a_i(s')\rangle = -\frac{\int_o^L G_{\rm hh}(s,s_1)ds_1 \int_o^L G_{\rm hh}(s',s_2)ds_2}{\int_0^L \int_0^L G_{\rm hh}(s_1,s_2)ds_1 ds_2} + G_{\rm hh}(s,s'). \tag{15}$$

If no motor is attached to the filament, the force-extension is explicitly given by

$$\langle R\rangle_{\rm WLC} = L - \frac{L^2}{2l_p}\left(\frac{\coth(\tilde{f}_{\rm ext})}{\tilde{f}_{\rm ext}} - \frac{1}{\tilde{f}_{\rm ext}^2}\right). \tag{16}$$

For small forces, the filament behaves like a spring,

$$f_{\rm ext} = k_{\parallel}^{\rm hh}(L)(L_r - \langle R\rangle), \tag{17}$$

with rest length $L_r = L - L^2/(6l_p)$ and a length dependent stiffness $k_{\parallel}^{\rm hh}(L) = \frac{90(l_p)^2}{\beta L^4}$.

IV. RESULTS

The explicit analytic solution for the Green function is given in the appendix. As a result, we obtain analytic, albeit lengthy expressions for the force extension $\langle R\rangle = \langle R\rangle(f_{\rm ext})$. To better understand these results, we plot the force-extension relations

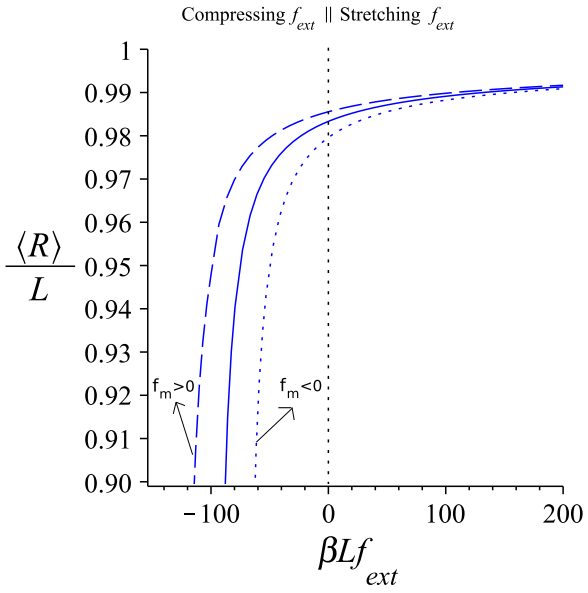

FIG. 2. Extension of the filament, $\langle R\rangle$, as a function of the external force $f_{\rm ext}$, which can be compressive or extensile; full line, no motor attached; dashed line, $\beta L f_m = +50$; dotted line, $\beta L f_m = -50$. (Parameters: $L = 1$, $l_p = 10$, $L/L_m = 2$; hinged-hinged filament.)

for hinged-hinged boundary conditions in Fig. 2. The effect of the motor force is more pronounced in the compressional regime, $f_{\rm ext} < 0$, because the filament is softer in response to compressions as compared to extensions, $f_{\rm ext} > 0$. The motor force can partially compensate the compression of the fiber by the external force, if its sign is opposite, i.e., it is pulling on the left part of the segment. Obviously, the left segment is then extended as compared to the case without motor (see Fig. 3, upper part), but also the right segment is extended (see Fig. 3, lower part), even though the tension in the right part does not depend on f_m. The reason for this extension is the stronger alignment of the left end of the right part of the filament by the motor. The overall effect of a positive motor force is to substantially stiffen the filament in the compressional regime. The effects, of course, increase with increasing motor force. If the motor force is compressional the extension of the filament is correspondingly reduced as compared to the case without motor force.

In Fig. 4, we show the dependence of the filaments extension on the motor force, f_m, for several values of external pulling force, $f_{\rm ext}$. If no external force is applied $\langle R\rangle = \langle R\rangle(f_m)$ looks qualitatively similar to $\langle R\rangle = \langle R\rangle(f_{\rm ext})$. The filament is most sensitive to the external pulling force in the range where the motor tends to compress the filament.

The effects of the motor are seen best in the differential tensile stiffness of the filament, which can be computed from the force-extension relation according to

$$E^{-1} = \frac{\partial\langle R\rangle}{\partial f_{\rm ext}}. \tag{18}$$

In Fig. 5 we show the relative change in the differential stiffness of the filament caused by the spring. There is significant enhancement in stiffness when the spring force is extensile (dashed line), because the effective tension of the filament is

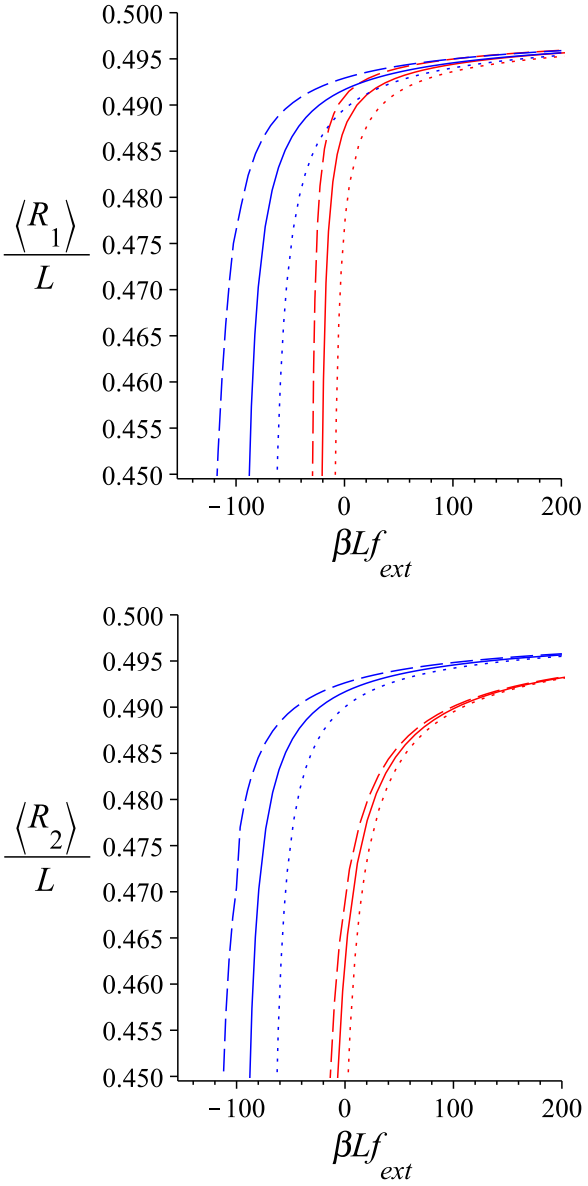

FIG. 3. Extension of the two separate parts of the filament, $\langle R_1 \rangle$ and $\langle R_2 \rangle$, as a function of the external force, $f_{\rm ext}$, for several values of the motor force; red lines, clamped-free filament; blue lines, hinged-hinged filament. (Full lines, no motor attached; dashed lines, $\beta L f_m = +50$; dotted lines, $\beta L f_m = -50$; parameters as described in the caption of Fig. 2.)

increased. The stiffness is weakened for a compressive motor force (full lines). In both cases do we observe stronger effects in the regime where the external force is compressive, implying that a filament under compression is strongly sensitive to a motor which is either pushing or pulling.

A. Limit of small motor force f_m

It is instructive to consider the limit of small motor force $f_m \ll \min\{f_{\rm ext}, \frac{\kappa}{L^2}\}$. For the clamped-free case, we find

$$\langle R \rangle - \langle R \rangle_{f_m=0} = \frac{f_m}{k(f_{\rm ext})}. \tag{19}$$

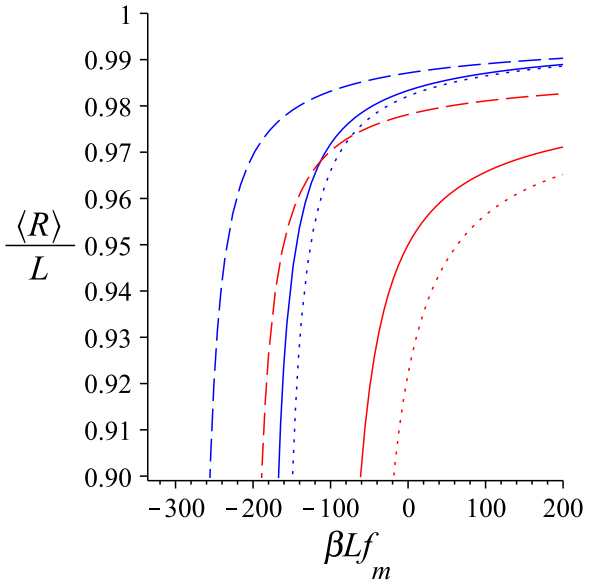

FIG. 4. Extension of the filament, $\langle R \rangle$, as a function of the motor force f_m for several values of the external force; red lines, clamped-free filament; blue lines, hinged-hinged filament. (Full lines, no motor attached; dashed lines, $\beta L f_{\rm ext} = +50$; dotted lines, $\beta L f_{\rm ext} = -10$; parameters as described in the caption of Fig. 2.)

In this limit, the motor-filament system can be represented as a linear elastic element with an effective force constant k that depends on the external pulling force and the point of attachment of the motor. The explicit expression for the force constant is given in the Appendix, and a similar expression can be calculated for the hinged-hinged case. In Fig. 6, we show the force constant k of the motor as a function of the external

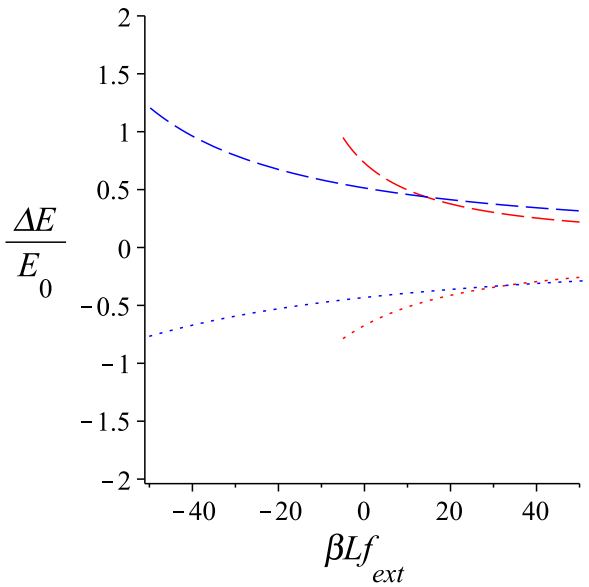

FIG. 5. Change in the differential stiffness relative to the case without a spring as a function of the external force; red lines, clamped-free filament; blue lines, hinged-hinged filamen. (Dashed lines, $\beta L f_m = +50$; dotted lines, $\beta L f_m = -50$; parameters as described in the caption of Fig. 2.)

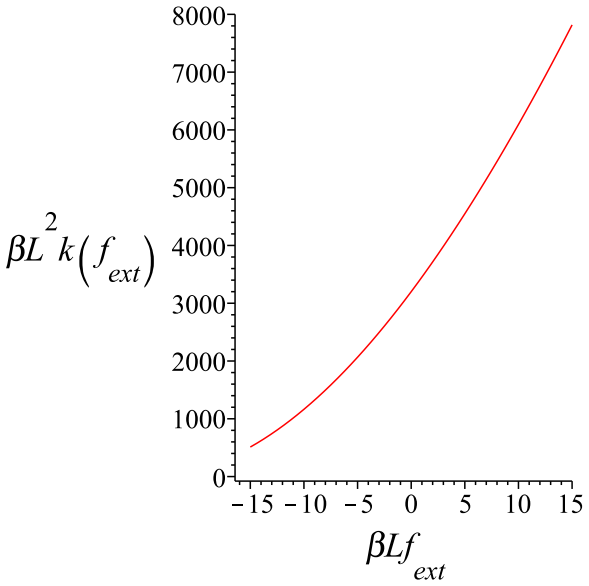

FIG. 6. Effective stiffness, $k(f_{\rm ext})$, of the filament with respect to the motor force as a function of external force $f_{\rm ext}$. The range of the external force is chosen in a way that the filament is well approximated as weakly bending ($\frac{R}{L} > 0.9$); parameters as described in the caption of Fig. 2.

force $f_{\rm ext}$. The force constant decreases as we compress the filament and it increases as we increase the stretching force. This change of the motor force constant k is an essential feature of the elasticity of the semiflexible filament which is missing in studies using linear elasticity for the filament. In Fig. 7, we compare the exact force-extension relation to the linearised one. As can be seen in the figure, the linear approximation works better for higher values of the external force $f_{\rm ext}$.

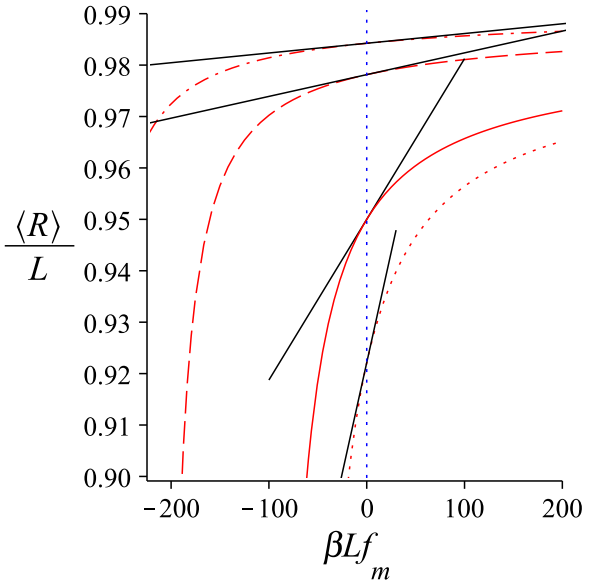

FIG. 7. Comparison of the complete solution for the end-to-end distance $\langle R\rangle/L$ and the one linearized around $f_m = 0$; full lines, $\beta L f_{\rm ext} = 0$; dashed lines, $\beta L f_{\rm ext} = 50$; dashed-dotted lines, $\beta L f_{\rm ext} = 100$; dotted line, $\beta L f_{\rm ext} = -10$; parameters as described in the caption of Fig. 2.

In the limit of large external forces, $f_{\rm ext} \gg \max\{f_m, \frac{\kappa}{L_m^2}\}$, and large filament length, $\min\{L, L_m\} \gg f_{\rm ext}/(k_B T)$, Eq. (19) reduces to the following relation, irrespective of boundary conditions:

$$\frac{\langle R\rangle}{L} = 1 - \frac{1}{2}\frac{k_B T}{\sqrt{\kappa f_{\rm ext}}} + \frac{L_m}{4L}\frac{k_B T f_m}{\sqrt{\kappa}\, f_{\rm ext}^{\frac{3}{2}}}. \tag{20}$$

Notice that this equation holds in the thermodynamic limit and it is scale invariant: if we multiply all lengths ($\langle R\rangle$, L_m, L) by the same factor, it does not change. The effect of the motor force is subdominant, as it scales with $\sim 1/f_{\rm ext}^{3/2}$ compared to $\sim 1/\sqrt{f_{\rm ext}}$ for the Marko-Siggia case, but it is noteworthy that it persists in the thermodynamic limit and is not just a finite-size effect.

In the limit of small external forces, $f_{\rm ext} \ll \kappa/L^2$, we obtain a linear response to both the motor and the external force, which in the case of clamped-free boundary conditions reads

$$\frac{\langle R\rangle_{\rm cf}}{L} = 1 - \frac{L}{2l_p} + \frac{2L_m^3 L - L_m^4}{6L^3 l_p}\tilde{f}_m + \frac{L}{6l_p}\tilde{f}_{\rm ext}. \tag{21}$$

B. Limit of large motor force f_m

In the limit of large motor force, $f_m \gg \max\{f_{\rm ext}, \frac{\kappa}{L_m^2}\}$, we expect the left part of the filament to display the asymptotic (Marko-Siggia) force extension for large f_m and indeed it does:

$$\langle R_1\rangle_{\rm cf} = L_m - \frac{L_m}{2l_p}\sqrt{\frac{\kappa}{f_m}}. \tag{22}$$

However, the extension of the right part of the filament is not just given by the expression for a wormlike chain under tension $f_{\rm ext}$ but shows a correction of $\mathcal{O}(\frac{1}{\sqrt{f_m}})$:

$$\langle R_2\rangle_{\rm cf} = \langle R_2\rangle_{\rm WLC} - \alpha(f_{\rm ext})\sqrt{\frac{\kappa}{f_m}}. \tag{23}$$

The strength of the effect depends on the external pulling force (see Fig. 8) and is strongest for weak pulling force. Explicit forms of $\langle R_2\rangle_{\rm WLC}$ and $\alpha(f_{\rm ext})$ are given in the Appendix.

In the limit of small external force, $f_{\rm ext} \ll \kappa/L^2 \ll f_m$ and $\kappa/L_m^2 \ll f_m$, we obtain a linear force-extension relation:

$$\frac{\langle R\rangle_{\rm cf}}{L} = 1 - \frac{L}{2l_p} + \frac{L_m(6L - 3L_m)}{6l_p L} + \frac{(L - L_m)^4}{6L^3 l_p}\tilde{f}_{\rm ext} - \frac{(6L - 3L_m)L_m}{6l_p L}\frac{1}{\tilde{f}_m^{\frac{1}{2}}}. \tag{24}$$

C. Limit of large force $f_{\rm ext}$ and $f_m = -f_{\rm ext} + \epsilon$

Next, we consider the limit of a large external pulling force, which is almost compensated by the motor in the left part of the filament. In other words, we put $f_m = -f_{\rm ext} + \epsilon$ and consider the case with $f_{\rm ext} \gg \frac{\kappa}{L_m^2}$ and $\epsilon \ll \frac{\kappa}{L^2}$. In this limit, the right part of the filament is asymptotically extended,

$$\langle R_2\rangle_{\rm cf} = L - L_m - \left(\frac{L - L_m}{2l_p}\right)\left(\frac{\kappa}{f_{\rm ext}}\right)^{1/2}. \tag{25}$$

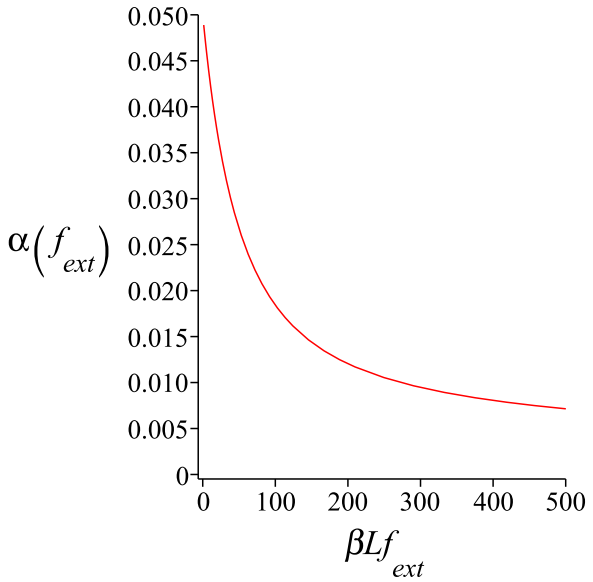

FIG. 8. Coefficient of the asymptotic expansion, $\alpha(f_{\rm ext})$, as function of external force $f_{\rm ext}$; parameters as described in the caption of Fig. 2.

The total extension in this limit is given by

$$\langle R\rangle_{\rm cf} - L = \frac{L_m^2}{6l_p} - \left(\frac{L}{6l_p}\right)\frac{(3L - L_m)}{\tilde{f}_{\rm ext}^{\frac{1}{2}}} + \left(\frac{L_m^4}{90 l_p L^2}\right)\frac{\epsilon L^2}{\kappa}. \tag{26}$$

The first term accounts for the reduction in length due to thermal fluctuations in the left part only and hence $\propto L_m^2$. The tension in the left part is just $\epsilon \ll 1$, which accounts for the last term. However, the pulling force $f_{\rm ext}$ affects the orientation of the tangent at L_m and hence also the extension of the left part of the filament so the dominant term for strong pulling force is not just determined by the right part of the filament.

V. RELATION TO SINGLE-MOTOR EXPERIMENTS

Our results can be tested experimentally using optical tweezers. Beads attached to the two ends of the biomolecule, which acts as track (e.g., F-actin), are trapped with optical tweezers. The motor (e.g., myosin-V) is attached with one end to a fixed bead and with the other end to the filament. Since the two end beads are free to rotate, this arrangement corresponds to the case of hinged-hinged boundary conditions. This experimental setup has already been used in many single-molecule mechanical transducers [10]. The "three-bead" technique was pioneered by Finer *et al.* [18]. The main idea is to measure the variance of the end-beads' position, which is related to the stiffness of the actomyosin cross-bridge complex within linear elasticity [19,20]. Conformational changes in the motor induce changes in the effective stiffness of the bridge, which is measured experimentally. In our model, the conformational change in myosin changes the motor force f_m. This can be due to a change in the position of attachment of the myosin head on the actin filament, L_m, or a change in the effective spring constant, k_m, or both.

Our results have been obtained in the fixed force ensemble, where the tension on the filament is determined sharply and this results in a fluctuating extension, whose average we have calculated. The positions of the motor bead, which determines X_0 in our model, and of the left filament end are held fixed. This can be done by using a very stiff optical trap. As shown by Gerland *et al.* in Ref. [21], a polymer held between two optical traps is represented by the mixed ensemble, where both the tension and the extension fluctuate. This mixed ensemble interpolates between the fixed extension ensemble (corresponding to the limit of very stiff traps) and fixed force ensemble (corresponding to the limit of very soft traps). Therefore, our general results for hinged-hinged boundary conditions can be tested with a setup involving a very soft optical trap for the right end of the filament. We should point out that the force-extension relation given by Eq. (20) holds in the thermodynamic limit and as such is ensemble independent (fixed force or fixed extension). In addition, the linear response results are ensemble independent.

In real systems, the spring will act not only in the longitudinal direction but also in the transverse direction. The effect of a transverse spring of zero rest length in the force-extension relation of a weakly bending wormlike chain has been calculated in Ref. [22]. For a spring of finite rest length, which is almost parallel to the longitudinal direction of the filament, the transverse effect is of higher order and can be neglected. For a spring of zero rest length but with $f_m \neq 0$, we can simply add the following contribution to the right-hand side of Eq. (20):

$$\frac{\Delta\langle R\rangle}{L} = \frac{k_m k_B T}{4 f_{\rm ext}^2}\left(1 + \frac{k_m L}{2 f_{\rm ext}}\right)^{-1}, \tag{27}$$

which holds in the strong stretching limit, $f \gg \kappa/L_m^2$. For a soft spring, $k_m L \ll f_{\rm ext}$, this contribution falls off as $\sim f_{\rm ext}^{-2}$, which is subdominant to the longitudinal contribution, which falls off as $\sim f_{\rm ext}^{-3/2}$.

VI. CONCLUSION AND OUTLOOK

We have analyzed the force-extension of a wormlike chain whose one end is fixed, while the other end is pulled or pushed by an external force. In addition, the filament is attached to a spring, which may represent a cross-link or a motor arrested at its stall force. Irrespective of boundary conditions, the effects of the spring are stronger in the compressive regime as compared to the stretching regime. Depending on the relative sign of the pulling force and the spring force, the latter can substantially stiffen or weaken the filament. When the motor force is small, its effects can be represented by an effective spring constant, which strongly depends on the prestress of the fiber, i.e., the external force. When the motor force is large, it gives rise to the same $1/\sqrt{f_{\rm ext}}$ dependence, which is well known from the work of Marko and Siggia [14].

The dependence of the force extension curve of the filament on motor force allows us to deduce the latter from measurements of the force-extension relation. In fact, the so-called three-bead geometry has already been used to determine the stiffness of the actomyosin cross-bridge [20].

An interesting direction for future work is the study of two or more parallel-aligned filaments with nonlocal springlike cross-linkers in the direction of alignment. The case of local

cross-links has been investigated in Refs. [22–24]. A simplified model of two filaments with a nonlocal spring has been studied in Ref. [25].

ACKNOWLEDGMENT

We thank the DFG for financial support through Grant No. SFB 937, Project A1.

APPENDIX

1. Filament with hinged-hinged boundary conditions at the two tips

The force is a piecewise constant function with two pieces. As result of this fact, the Green function is a piecewise function with six pieces:

$$G(s,s') = \begin{cases} G_1^-(s,s') & 0 < s < s' \leqslant L_m < L \\ G_1^+(s,s') & 0 < s' < s \leqslant L_m < L \\ G_2^-(s,s') & 0 < L_m \leqslant s < s' < L \\ G_2^+(s,s') & 0 < L_m \leqslant s' < s < L \\ G_3^-(s,s') & 0 < s < L_m < s' < L \\ G_3^+(s,s') & 0 < s' < L_m < s < L \end{cases}. \tag{A1}$$

The assumption that the derivative of the tangent vector is zero at the end tips (hinged-hinged condition) leads to the vanishing of the derivative of the Green function. Considering the boundary conditions, the solution for the aforementioned equation must have the following form:

$$G_{\mathrm{hh}}(s,s') = \begin{cases} G_1^-(s,s') = N_{11}(s')\cosh(s\sigma_1) \\ G_1^+(s,s') = N_{12}(s')[\cosh(s\sigma_1) + A_1\sinh(s\sigma_1)] \\ G_2^-(s,s') = N_{21}(s')[\cosh(s\sigma_2) + A_2\sinh(s\sigma_2)] \\ G_2^+(s,s') = N_{22}(s')\cosh((L-s)\sigma_2) \\ G_3^-(s,s') = N_{31}(s')\cosh(s\sigma_1) \\ G_3^+(s,s') = N_{32}(s')\cosh[(L-s)\sigma_2] \end{cases}, \tag{A2}$$

where $\sigma(s) = \sqrt{\frac{f(s)}{\kappa}} = \{^{\sigma_1 = \sqrt{\frac{f_1}{\kappa}} \quad 0 < s < L_m}_{\sigma_2 = \sqrt{\frac{f_2}{\kappa}} \quad L_m < s < L}$ and L_m is the position of molecular motor in terms of the contour length. Moreover, constants appearing in Eq. (A2) are obtained from the following conditions:

$$\begin{aligned} \frac{\partial G_1^+(s,s')}{\partial s}\,|_{s=s'} - \frac{\partial G_1^-(s,s')}{\partial s}\,|_{s=s'} &= -\frac{1}{\beta\kappa}(1) \\ G_1^-(s',s') &= G_1^+(s',s') \quad (2) \\ \frac{\partial G_2^+(s,s')}{\partial s}\,|_{s=s'} - \frac{\partial G_2^-(s,s')}{\partial s}\,|_{s=s'} &= -\frac{1}{\beta\kappa}(3) \\ G_2^-(s',s') &= G_2^+(s',s') \quad (4) \\ G_3^-(L_m,s') &= G_2^-(L_m,s') \quad (5) \\ G_3^+(L_m,s') &= G_1^+(L_m,s') \quad (6) \\ \frac{\partial G_3^-(s,s')}{\partial s}\,|_{s=L_m} &= \frac{\partial G_2^-(s,s')}{\partial s}\,|_{s=L_m} \quad (7) \\ \frac{\partial G_3^+(s,s')}{\partial s}\,|_{s=L_m} &= \frac{\partial G_1^+(s,s')}{\partial s}\,|_{s=L_m} \quad (8). \end{aligned} \tag{A3}$$

These conditions coming in Eq. (A3), except numbers (7) and (8), give

$$\begin{cases} N_{11}(s') = -\dfrac{\cosh(\sigma_1 s') + A_1 \sinh(\sigma_1 s')}{\sigma_1 l_p A_1} \\ N_{12}(s') = -\dfrac{\cosh(\sigma_1 s')}{\sigma_1 l_p A_1} \\ N_{21}(s') = \dfrac{\cosh[\sigma_2(L-s')]}{\sigma_2 l_p[\sinh(\sigma_2 L) + A_2 \cosh(\sigma_2 L)]} \\ N_{22}(s') = \dfrac{\cosh(\sigma_2 s') + A_2 \sinh(\sigma_2 s')}{\sigma_2 l_p[\sinh(\sigma_2 L) + A_2 \cosh(\sigma_2 L)]} \\ N_{31}(s') = \dfrac{\cosh\{\sigma_2(L-s')[\cosh(\sigma_2 L_m) + A_2 \sinh(\sigma_2 L_m)]\}}{\sigma_2 l_p \cosh(\sigma_1 L_m)[\sinh(\sigma_2 L) + A_2 \cosh(\sigma_2 L)]} \\ N_{32}(s') = -\dfrac{\cosh(\sigma_1 s')[\cosh(\sigma_1 L_m) + A_1 \sinh(\sigma_1 L_m)]}{\sigma_1 l_p A_1 \cosh[\sigma_2(L-L_m)]} \end{cases}. \tag{A4}$$

Condition numbers (7) and (8) of Eq. (A3) give

$$\begin{cases} A_1 = -\dfrac{\sigma_2 \sinh[\sigma_2(L-L_m)]\cosh(\sigma_1 L_m) + \sigma_1 \sinh(\sigma_1 L_m)\cosh[\sigma_2(L-L_m)]}{\sigma_2 \sinh[\sigma_2(L-L_m)]\sinh(\sigma_1 L_m) + \sigma_1 \cosh(\sigma_1 L_m)\cosh[\sigma_2(L-L_m)]} \\ A_2 = -\dfrac{\sigma_1 \sinh(\sigma_1 L_m)\cosh(\sigma_2 L_m) - \sigma_2 \sinh(\sigma_2 L_m)\cosh(\sigma_1 L_m)}{\sigma_1 \sinh(\sigma_1 L_m)\sinh(\sigma_2 L_m) - \sigma_2 \cosh(\sigma_2 L_m)\cosh(\sigma_1 L_m)} \end{cases}. \tag{A5}$$

Concerning the boundary condition, the correlation function of the transverse components of tangent vector is written as follows:

$$\langle a_i(s) a_i(s') \rangle_{\mathrm{hh}} = \lim_{J_i \to 0} \frac{\delta^2 \ln[Z(J_i)]}{\delta J_i(s) \delta J_i(s')}, \tag{A6}$$

where $Z(J_i) = \int D\{a_i(s)\} \delta(\int_0^L ds a_i(s)) \exp(-\beta H_{\mathrm{WBA}} + \int_0^L ds J_i(s) a_i(s))$ is the generating functional with source term $J_i(s)$ and $\beta = \frac{1}{k_B T}$. The correlation function of the transverse components of the tangent vector is obtained by the following expression [16,17]:

$$\langle a_i(s) a_i(s') \rangle = G_{\mathrm{hh}}(s,s') - \frac{\int_o^L G_{\mathrm{hh}}(s,s_1) ds_1 \int_o^L G_{\mathrm{hh}}(s',s_2) ds_2}{\int_0^L \int_0^L G_{\mathrm{hh}}(s_1,s_2) ds_1 ds_2}, \tag{A7}$$

which implies

$$\langle {a_i}^2(s) \rangle = G_{\mathrm{hh}}(s,s) - \frac{\left[\int_o^L G_{\mathrm{hh}}(s,s_1) ds_1\right]^2}{\int_0^L \int_0^L G_{\mathrm{hh}}(s_1,s_2) ds_1 ds_2}. \tag{A8}$$

2. Filament with clamped-free boundary conditions at the two end tips

In the clamped-free case, we enforce the transverse components of the tangent vector of the filament at $s = 0$ and their derivative at $s = L$ to be zero. Similar to Appendix A, we obtain the following expression for the Green function:

$$G_{\mathrm{cf}}(s,s') = \begin{cases} G_1^-(s,s') \equiv \dfrac{\sinh(\sigma_1 s)[B_1 \cosh(\sigma_1 s') + \sinh(\sigma_1 s')]}{l_p \sigma_1 B_1} \\ G_1^+(s,s') \equiv \dfrac{[B_1 \cosh(\sigma_1 s) + \sinh(\sigma_1 s)]\sinh(\sigma_1 s')}{l_p \sigma_1 B_1} \\ G_2^-(s,s') \equiv \dfrac{\cosh[\sigma_2(L-s')][B_2 \cosh(\sigma_2 s) + \sinh(\sigma_2 s)]}{l_p \sigma_2 B_2 \sinh(\sigma_2 L) + l_p \sigma_2 \cosh(\sigma_2 L)} \\ G_2^+(s,s') \equiv \dfrac{\cosh(\sigma_2 s)[B_2 \cosh(\sigma_2 s') + \sinh(\sigma_2 s')]}{l_p \sigma_2 B_2 \sinh(\sigma_2 L) + l_p \sigma_2 \cosh(\sigma_2 L)} \\ G_3^-(s,s') \equiv \dfrac{\sinh(\sigma_1 s)\cosh[\sigma_2(L-s')][B_2 \cosh(\sigma_2 L_m) + \sinh(\sigma_2 L_m)]}{l_p \sigma_2 \sinh(\sigma_1 L_m)(B_2 \sinh(\sigma_2 L) + \cosh(\sigma_2 L))} \\ G_3^+(s,s') \equiv \dfrac{\cosh[\sigma_2(L-s)]\sinh(\sigma_1 s')[B_1 \cosh(\sigma_1 L_m) + \sinh(\sigma_1 L_m)]}{l_p \sigma_1 B_1 \cosh[\sigma_2(L-L_m)]} \end{cases}, \tag{A9}$$

where

$$\begin{cases} B_1 = -\dfrac{\sigma_2 \sinh[\sigma_2(L-L_m)]\sinh(\sigma_1 L_m) + \sigma_1 \cosh[\sigma_2(L-L_m)]\cosh(\sigma_1 L_m)}{\sigma_2 \sinh[\sigma_2(L-L_m)]\cosh(\sigma_1 L_m) + \sigma_1 \cosh[\sigma_2(L-L_m)]\sinh(\sigma_1 L_m)} \\ B_2 = \dfrac{\sigma_1 \cosh(\sigma_1 L_m)\sinh(\sigma_2 L_m) - \sigma_2 \sinh(\sigma_1 L_m)\cosh(\sigma_2 L_m)}{\sigma_2 \sinh(\sigma_1 L_m)\sinh(\sigma_2 L_m) - \sigma_1 \cosh(\sigma_1 L_m)\cosh(\sigma_2 L_m)} \end{cases}. \tag{A10}$$

The correlation function [16,17] is obtained as follows:

$$\langle a_i(s) a_i(s') \rangle_{\rm cf} = G_{\rm cf}(s,s'), \tag{A11}$$

which implies

$$\langle a_i^2(s) \rangle_{\rm cf} = G_{\rm cf}(s,s). \tag{A12}$$

3. Linear end-to-end distance in terms of f_m

The end-to-end distance of the whole filament when it is in the clamped-free condition can be written as follows:

$$\langle R \rangle_{\rm cf} = L - \frac{L^2 \tanh(\tilde{f}_{\rm ext}^{\frac{1}{2}})}{2 l_p \tilde{f}_{\rm ext}} + \left[\frac{1}{k(f_{\rm ext})}\right] f_m. \tag{A13}$$

The effective linear motor force constant k is

$$\begin{aligned} \frac{1}{k} = & -\frac{1}{4\left[l_p \kappa (\frac{f_{\rm ext}}{\kappa})^{\frac{5}{2}} (e^{4L\sqrt{\frac{f_{\rm ext}}{\kappa}}} + 2e^{2L\sqrt{\frac{f_{\rm ext}}{\kappa}}} + 1)\right]} \\ & \times \left[A e^{4L\sqrt{\frac{f_{\rm ext}}{\kappa}}} + B e^{2(2L-L_m)\sqrt{\frac{f_{\rm ext}}{\kappa}}} + C e^{2L\sqrt{\frac{f_{\rm ext}}{\kappa}}} + + D e^{2(L+L_m)\sqrt{\frac{f_{\rm ext}}{\kappa}}} + E e^{2(L-L_m)\sqrt{\frac{f_{\rm ext}}{\kappa}}} + F e^{2L_m\sqrt{\frac{f_{\rm ext}}{\kappa}}} + G\right], \end{aligned} \tag{A14}$$

where $A = -\frac{f_{\rm ext} L_m}{\kappa} + \sqrt{\frac{f_{\rm ext}}{\kappa}}, B = -(\frac{f_{\rm ext} L_m}{\kappa} + \sqrt{\frac{f_{\rm ext}}{\kappa}}), C = (\frac{4 f_{\rm ext} L L_m}{\kappa} + 2)\sqrt{\frac{f_{\rm ext}}{\kappa}}, D = -(\sqrt{\frac{f_{\rm ext}}{\kappa}} - \frac{f_{\rm ext} L_m}{\kappa} + \frac{f_{\rm ext} L}{\kappa}), E = -\sqrt{\frac{f_{\rm ext}}{\kappa}} - \frac{f_{\rm ext} L_m}{\kappa} + \frac{f_{\rm ext} L}{\kappa}, F = \frac{f_{\rm ext} L_m}{\kappa} - \sqrt{\frac{f_{\rm ext}}{\kappa}}, G = \frac{f_{\rm ext} L_m}{\kappa} + \sqrt{\frac{f_{\rm ext}}{\kappa}}$.

4. Limit of large motor force f_m

In the limit of large motor forces $f_m \gg \text{Max}\{f_{\rm ext}, \frac{\kappa}{L^2}\}$, we have the following expression for the end-to-end distance of the first piece of the filament,

$$\langle R_1 \rangle_{\rm cf} = L_m - \frac{L_m}{2 l_p}\sqrt{\frac{\kappa}{f_m}}, \tag{A15}$$

and the end-to-end distance of the second piece of the filament,

$$\langle R_2 \rangle_{\rm cf} = (L - L_m) - \frac{(L-L_m)}{2 l_p} \frac{\tanh\left((L-L_m)\sqrt{\frac{f_{\rm ext}}{\kappa}}\right)}{\sqrt{\frac{f_{\rm ext}}{\kappa}}} - \alpha(f_{\rm ext})\sqrt{\frac{\kappa}{f_m}}, \tag{A16}$$

where

$$\alpha(f_{\rm ext}) = \frac{e^{4L\sqrt{\frac{f_{\rm ext}}{\kappa}}} - e^{4L_m\sqrt{\frac{f_{\rm ext}}{\kappa}}}}{2 l_p \sqrt{\frac{f_{\rm ext}}{\kappa}}\left(e^{2L\sqrt{\frac{f_{\rm ext}}{\kappa}}} + e^{2L_m\sqrt{\frac{f_{\rm ext}}{\kappa}}}\right)^2} + \frac{2(L-L_m)e^{2(L+L_m)\sqrt{\frac{f_{\rm ext}}{\kappa}}}}{l_p\left(e^{2L\sqrt{\frac{f_{\rm ext}}{\kappa}}} + e^{2L_m\sqrt{\frac{f_{\rm ext}}{\kappa}}}\right)^2}. \tag{A17}$$

[1] Adam J. Engler, Shamik Sen, H. Lee Sweeney, and Dennis E. Discher, Matrix elasticity directs stem cell lineage specification, Cell **126**, 677 (2006).

[2] Darci T. Butcher, Tamara Alliston, and Valerie M. Weaver, A tense situation: Forcing tumour progression, Nat. Rev. Cancer **9**, 108 (2009).

[3] Tadanori Mammoto and Donald E. Ingber, Mechanical control of tissue and organ development, Development **137**, 1407 (2010).

[4] A. R. Bausch and K. Kroy, A bottom-up approach to cell mechanics, Nat. Phys. **2**, 231 (2006).

[5] Robyn H. Pritchard, Yan Yan Shery Huang, and Eugene M. Terentjev, Mechanics of biological networks: From the cell cytoskeleton to connective tissue, Soft Matter **10**, 1864 (2014).

[6] C. P. Broedersz and F. C. MacKintosh, Modeling semiflexible polymer networks, Rev. Mod. Phys. **86**, 995 (2014).

[7] Oliver Lieleg, Mireille M. A. E. Claessens, and Andreas R. Bausch, Structure and dynamics of cross-linked actin networks, Soft Matter **6**, 218 (2010).
[8] Steven J. Winder and Kathryn R. Ayscough, Actin-binding proteins, J. Cell Sci. **118**, 651 (2005).
[9] Eckhard Mandelkow and Eva-Maria Mandelkow, Microtubules and microtubule-associated proteins, Curr. Opin. Cell Biol. **7**, 72 (1995).
[10] Claudia Veigel and Christoph F. Schmidt, Moving into the cell: Single-molecule studies of molecular motors in complex environments, Nat. Rev. Mol. Cell Biol. **12**, 163 (2011).
[11] Erika L. F. Holzbaur and Yale E. Goldman, Coordination of molecular motors: From *in vitro* assays to intracellular dynamics, Curr. Opin. Cell Biol. **22**, 4 (2010).
[12] A. F. Huxley, Muscle structure and theories of contraction, Prog. Biophys. Biophys. Chem. **7**, 255 (1957).
[13] Thomas Guérin, Jacques Prost, Pascal Martin, and Jean-François Joanny, Coordination and collective properties of molecular motors: Theory, Curr. Opin. Cell Biol. **22**, 14 (2010).
[14] John F. Marko and Eric D. Siggia, Stretching DNA, Macromolecules **28**, 8759 (1995).
[15] Azam Gholami, Jan Wilhelm, and Erwin Frey, Entropic forces generated by grafted semiflexible polymers, Phys. Rev. E **74**, 041803 (2006).
[16] Yuko Hori, Ashok Prasad, and Jané Kondev, Stretching short biopolymers by fields and forces, Phys. Rev. E **75**, 041904, (2007).
[17] Michael E. Peskin and Daniel V. Schroeder, *An Introduction to Quantum Field Theory* (Westview, Boulder, CO, 1995).
[18] Jeffrey T. Finer, Robert M. Simmons, and James A. Spudich, Single myosin molecule mechanics: Piconewton forces and nanometer steps, Nature **368**, 113 (1994).
[19] Claudia Veigel, Fei Wang, Marc L. Bartoo, James R. Sellers, and Justin E. Molloy, The gated gait of the processive molecular motor, myosin V, Nat. Cell Biol. **4**, 59 (2002).
[20] Claudia Veigel, Marc L. Bartoo, David C. S. White, John C. Sparrow, and Justin E. Molloy, The stiffness of rabbit skeletal actomyosin cross-bridges determined with an optical tweezers transducer, Biophys. J. **75**, 1424 (1998).
[21] Ulrich Gerland, Ralf Bundschuh, and Terence Hwa, Mechanically probing the folding pathway of single RNA molecules, Biophys. J. **84**, 2831 (2003).
[22] Panayotis Benetatos, Stephan Ulrich, and Annette Zippelius, Force-extension relation of cross-linked anisotropic polymer networks, New J. Phys. **14**, 115011 (2012).
[23] Alice von der Heydt, Daniel Wilkin, Panayotis Benetatos, and Annette Zippelius, Elasticity of cross-linked semiflexible biopolymers under tension, Phys. Rev. E **88**, 032701 (2013).
[24] Panayotis Benetatos, Alice von der Heydt, and Annette Zippelius, Tension-induced binding of semiflexible biopolymers, New J. Phys. **16**, 113037 (2014).
[25] T. B. Liverpool, M. C. Marchetti, J.-F. Joanny, and J. Prost, Mechanical response of active gels, Europhys. Lett. **85**, 18007 (2009).